



Fermi National Accelerator Laboratory

FERMILAB-Conf-91/281

Physics Requirements for LHC/SSC Calorimetry

D. Green

*Fermi National Accelerator Laboratory
P.O. Box 500, Batavia, Illinois 60510*

October 1991

* Presented at the *Calorimetry and High Energy Physics Conference*, Capri, Italy, October 14-18, 1991.



PHYSICS REQUIREMENTS FOR LHC/SSC CALORIMETRY

DAN GREEN
Fermi National Accelerator Laboratory
P.O. BOX 500
Batavia, Illinois 60510, USA

1. Introduction

The goal of the next generation of collider detectors is to study the origin of electroweak symmetry breaking. The mass scale for this study is roughly 1 TeV. No matter what the details of the mechanism, one can be confident that new phenomena will occur, since weak interactions become strong, i.e. violate partial wave unitarity, at that mass scale [1]. The partial wave amplitude for $ee \rightarrow WW$ scattering is;

$$a_0 \sim \frac{\alpha_w}{4\pi} \left(\frac{M}{M_W} \right)^2$$
$$a_0 \sim 1 \text{ if } M \sim 1 \text{ TeV} \quad (1)$$

Therefore, the detectors for LHC/SSC must be able to confront this mass scale. In particular, the electroweak dynamics is such that the study of gauge boson pairs has a high priority. Given that the simplest decay modes for gauge bosons are into leptons, the new detectors will naturally tend to optimize performance for leptons.

2. Physics Processes and Rates

Calorimetry will be the basis for the new detectors. It plays a role in identifying or measuring all the components of the Standard Model. Leptons appear as missing energy or electromagnetic (EM) showers, or minimum ionizing towers, or narrow jets for neutrinos, electrons, muons, or taus respectively. The quarks will appear as jets of particles. The gauge bosons will appear as EM showers, jets, or lepton pairs for photons, gluons, and W/Z respectively. The calorimeter measures the magnitude, position, and time of energy deposition over some angular range. The nonuniform response of the calorimeter to different particle species means that it also assists in particle identification. In addition, calorimetry is the technology which improves, or stays fractionally constant, with energy. Therefore, high energies are the natural province of calorimeters.

The weakness of the Higgs coupling to ordinary matter implies that the LHC/SSC detectors must operate at very high luminosities. The event rates will be in the range 100 to 1000 Mhz. The natural time scale for the calorimetry to respond is the rf bunch spacing of ~ 16 nsec. Some representative rates are given in Table 2.1. Much more detail may be found in the recent SDC study [2].

The rates are given as rough functions of P_t and integrated over P_t for all $P_t > 20$ GeV. The general angular coverage and P_t trigger threshold requirements can be seen from inspection of Fig. 1. Clearly a coverage in pseudorapidity, η , of $|\eta| < 3.0$ with

a trigger cut of $P_t > 20$ GeV is appropriate for good Higgs detection efficiency. Typical hard scattering rates, if dominated by dynamics and not quark/gluon source distributions, will fall as the inverse third power of P_t .

The singles rates in Table 2.1 vary from Jets at ~ 1 Mhz, to single pions at ~ 10 Khz, to gauge bosons at ~ 40 Hz. Note that the copious rate of $Z \rightarrow 2e$ allows one a source of tagged e for calibration of the calorimeters. The pairs are produced at reduced rates, the most copious being photon pairs. Pairs of W bosons come from top pair decays, while Z pairs are directly produced. The rates for gauge pairs are shown in Fig. 2.

From Table 2.1 one can immediately make some conclusions. The rate for ZZ with 1 Z decaying into ll and the other into $\nu\nu$ is ($P_t > 20$ GeV) ~ 0.0008 Hz. The rate for $Z + J$ is ~ 1 Hz. Therefore, one needs to find jets, J, with an efficiency of better than 1 part in 250. Comparing the JJ and $q\bar{q}$ rates, one sees that one must contain a jet to 1 part in 1/1000 in order that jet leakage not dominate heavy flavor sources of ν (= missing P_t). The relative rates for ZJ and ZZ lead to the requirements on coverage shown in Fig. 3. In order that the jet be tagged, coverage (with efficiency > 0.995) out to $|\eta| \sim 5$ is needed, if $Z \rightarrow \nu\nu$ decay modes are to be used in the physics analysis. Therefore, angular coverage to $|\eta| = 3$ is for triggering and reconstruction of leptons with good efficiency in $H \rightarrow ZZ$ and $\rightarrow 2$ gamma decays. Missing P_t in $Z \rightarrow \nu\nu$ requires coverage out to $|\eta|=5$.

The simulation of the physics processes of interest and the associated backgrounds leads to a set of requirements for the calorimeters, their measurements of energy, position, time, and particle ID properties [2]. A partial list of the salient requirements discussed in Ref. 2 is shown in Table 2.2. The parameter, the physics process, and the requirement on the parameter are shown in the Table. The issues of hermiticity, calibration, angular coverage, and trigger coverage have already been briefly raised. In what follows, details of the other entries in Table 2.2 will be given.

3. Hadronic Size and Segmentation

This section discusses the physics processes which are studied in making decisions about the size, longitudinal and transverse segmentation of the hadronic calorimeter.

3.1 Total Depth : Dijet Mass and Missing P_t

The depth of the calorimetry is a cost driver since it defines the total volume of material. The requirements have been extensively studied [3]. The physics driver is to have unimpaired dijet mass resolution at the highest accessible mass, about 10 TeV. That requires a total depth of about 10 absorption lengths in order to limit leakage fluctuations. A plot of mass resolution as a function of calorimeter total depth, D, in absorption lengths is shown in Fig. 4. Other subsidiary requirements are discussed in detail in Ref. 4. Suffice it to say that most of them cluster in the region of 10 absorption lengths. A scheme to weight the last sampling layer [5] allows one to shrink the depth by about 1, while retaining roughly constant resolution.

3.2 Weighting and Depth Reduction

In Fig. 5 is shown the contained energy for 0.45 TeV incident beam. One compares a depth of 10 for an unweighted calorimeter to a depth of 8.7 for a depth segmented weighted calorimeter. Clearly the rms in the two cases is very similar. The Gaussian part of the energy distribution is slightly wider, but a glance at Fig. 4 shows that the degradation is acceptable. Thus, in terms of resolution, a calorimeter with $D = 9$ is (barely) acceptable.

Nonlinearity is potentially an issue for a too thin calorimeter. The unweighted $D = 10.1$ version is linear up to 0.2 TeV and then leakage causes a $\sim 1\%$ nonlinearity at 0.45 TeV. The $D = 8.7$ weighted option, with weight = 3, overcorrects by 1% for $E < 0.3$ TeV, followed by 1% leakage at 0.45 TeV [3]. Therefore, the nonlinearity induced by weighting is acceptable given the required energy resolution.

3.3 Longitudinal Segmentation and Depth Reduction

The total depth was set by the Gaussian part of the dijet mass resolution. However, there are fluctuations in the hadronic shower development which lead to long non-Gaussian tails in the energy resolution. These may be controlled by segmenting the hadronic absorber into 2 compartments [4]. A plot of the containment energy fraction at a depth of 10.1 with and without longitudinal segmentation, at 0.45 TeV, is shown in Fig. 6. Clearly, control is needed in order that these tails not be the dominant contribution to the missing energy [6]. The optimal split is set by the desire to tag energy leaking out the back, taking into account that some hadronic showers have low energy deposition gaps in their development. A rear section of 3 to 4 absorption lengths appears to be optimal [4].

3.4 Transverse Segmentation : Dijet Mass and e ID

A study was made for the impact of Higgs bosons decaying into ZZ which subsequently decay into jets. The mass resolution for a Z from 0.8 TeV Higgs bosons is degraded for segmentation > 0.05 [3]. The desire is to preserve Z dijet mass resolution for boosted Z s. A plot of dijet mass resolution as a function of segmentation is shown in Fig. 7. Note that the effect in going from segmentation of 0.05 to 0.1 is not very large.

Given the importance of gauge boson pairs, and thus e , the impact of hadron segmentation on electrons must be kept in mind. For electron ID, isolation is a crucial cut variable. Segmentation defines how near a jet electrons may be defined. The hadronic segmentation of the first compartment may be chosen to match that of the EM compartment(s) so as to make triggering most graceful. This tower matching makes "EM/HAD" and "isolation" easy to impose and insures that electrons may be identified as close to jets as the EM segmentation allows. A recent study [7] indicates a loss in efficiency of $\sim 20\%$ in going from 0.05 hadron segmentation to 0.10 at design luminosity.

Finally, it must be kept in mind that the SSC can reach 10x of the design luminosity fairly easily. The energy deposited in a LHC tower goes as the area, and fluctuations in the pileup "noise" thus go as the segmentation. It seems prudent to allow for increases in luminosity by maintaining fine hadronic segmentation.

4. EM Size and Segmentation

The EM calorimeter parameters are set by the need to make a precise measurement of EM energy and by the necessity of good e ID [8]. The needs of particle identification largely define the EM segmentation.

4.1 Total Depth and Leakage

The depth requirement is set by the need to contain the highest $P_t e$ without inducing a "leakage error" which exceeds the intrinsic EM resolution. For 99% containment at 0.1 TeV, a ~ 25 radiation length, t , EM calorimeter is needed. In addition, since the fine segmentation is expensive, one can consider weighting the last layers of the EM calorimetry in exactly the same fashion as was discussed for the hadronic sections. Note that a very deep EM compartment would lose hadronic rejection and thus is not desirable in any case.

4.2 Weighting and Depth Reduction

An exit weighting scheme gives essentially the same resolution for a $t = 22$ calorimeter as a $t = 50$ EM calorimeter. Therefore, at least from the point of view of EM resolution and containment, weighting the last EM samples is acceptable. However, the impact on hadronic resolution of showers developing early in the EM section has not yet been evaluated. This weighting scheme is still under active study.

4.3 Longitudinal Segmentation and Radiation Damage

The electron compartment(s) naturally divide along the "shower maximum" boundary at about 6 radiation lengths. It is not deemed necessary to have longitudinal segmentation in order to do electron ID. The use of E/p , isolation, EM/HAD, transverse shower shapes, and shower max matching are sufficient [9]. The shower maximum detector serves as a second, redundant, measurement of EM energy which will allow for a check against grossly mismeasured energies (e.g. "sparks").

There is another virtue in longitudinal segmentation. In the endcap EM sections, the radiation field is intense. The implementation of 2 EM longitudinal compartments allows one to make an event by event measurement of shower initiation points, and hence to correct even severe damage to a level allowed by precision EM calorimetry specifications [10]. In Fig. 8 is shown the "induced" constant term for damage coefficients up to 50% for uncorrected and corrected (2 compartments) operation. Clearly, the method allows one to operate at up to 50% damage for isolated electrons since the error due to damage then is less than the resolution.

4.4 Transverse Segmentation and b Decays

One potential scale for EM transverse size is the Moliere radius. At a 2 m distance, this scale means segmentation of roughly 0.01. That size can be accommodated, in 1 dimension, by an array of crossed "shower maximum" strips for an affordable strip count. There are no other natural scales to point to. In Fig. 9 we show for $t \rightarrow W + b$, $b \rightarrow c + e + \nu$ events the ratio of electron energy to all energy, on average, in a cone of radius R as a function of R . The isolation falls as $1/R^2$. A 5% isolation, comparable to the e energy resolution in these events, implies a segmentation of roughly 0.035. Note that this estimate ignores the possibility of high

luminosity "minbias" pileup from overlapping events. This smooth background should be subtractable on average, leaving a fluctuation scaling as $1/R$.

4.5 Transverse Segmentation and e Track Matching

The shower centroid can be found accurately if the strips have a width of about the size of the Moliere radius. Therefore, crossed strip detectors with a width of 0.01 in azimuthal angle and rapidity are plausible.

What determines the strip length? Clearly, the centroid measurement will be degraded by pileup fluctuations. The centroid error should scale as the square root of the length. In Fig. 10 is shown the mean deviation in ϕ and η as a function of strip length for $t \rightarrow W + b$, $b \rightarrow c + e + \nu$ events. This error will define the cut limits for track matching with the SM centroid. The solid curve corresponds to square root (length), while the dashed curve is a smooth representation of the field on data. Setting a design criterion that the pileup error be $< 1/2$ the strip width, one finds that lengths of 0.5 are acceptable.

4.6 EM Segmentation and Jet Rejection

The JJ cross section far exceeds the cross section for e , as seen in Table 2.1. Typically an electron trigger requires $E_t > \text{threshold}$ in EM, $EM/HAD > 10$, and $EM/(E \text{ in "isolation" ring}) > 4$. These cuts are roughly 95% efficient [7]. A jet will pass the same set of cuts, $\sim 1/2000$ of the time. The rejection factor for jets scales roughly as the inverse of the EM linear segmentation. This scaling makes jet rejection by the use of finer segmentation fiscally difficult.

5. Hadronic Energy Resolution

5.1 Z Dijets and Resolution

As discussed above, some of the fundamental entities of the Standard Model will appear in the calorimeters as jets. What energy measurement accuracy is required? A study [11] of Z and 1 TeV Z' decaying into dijets at both high and low P_t was made to address this question. A summary of the results is shown in Fig. 11. Clearly, the major effects come about due to clustering algorithms and the underlying event. The effects of any reasonable HAD calorimeter resolution are minimal. Therefore, one concludes that precise hadronic energy resolution is not required in the hadronic compartment of the calorimeters.

5.2 Dijets and e/h

A continuation of the study referred to in section 5.1 was made to explore the e/h requirements in more detail [12]. The results of that study are summarized in Fig. 12. The fractional dijet mass resolution at masses up to 10 TeV is dominated by fluctuations in the fragmentation and the underlying event. Calorimeter resolution is less important. Neutrino fluctuations from heavy flavor decay within the jet begin to become more important than the resolution at the highest accessible masses.

Clearly, the difficulty in precisely defining a jet alleviates the strict requirements one might place on hadronic calorimetry. In Fig. 13 is shown the fractional dijet mass resolution as a function of mass. The comparison is between

$e/h=1$, $e/h=1.3$ with the EM and HAD compartments calibrated to equal response at all energies, and only at asymptotic energies. Obviously, $e/h < 1.3$ does not make a major impact on jet resolution.

5.3 Speed, Overlaps and Z Dijets

The weak coupling of the Higgs means that high luminosity machines are needed to confront Higgs physics. Thus, the issue of event pileup is of interest. A study has been made of event pileup for dijet decays of boosted Z [13]. Results for dijet mass resolution as a function of cone size, R , are shown in Fig. 14 for up to 16 overlapped minbias events. Without overlaps $R \sim 0.7$ is optimal and leads to minor increases in resolution due to fluctuations. The overlap of 16 events is partially controlled by placing a tower threshold of 2 GeV in Pt. However, the dijet mass resolution is still degraded by a factor ~ 2.5 with respect to the case with no overlapping events. Therefore, jet spectroscopy will be badly compromised at high luminosity. The resolution should worsen at the square root of the luminosity.

5.4 Uniformity Tolerance in Sampling Calorimeters

The specification on the tolerance for both the absorber and the active medium is driven by the resolution specification. For hadrons, a study [11] showed that for constant terms $< 3\%$, no adverse effects on jet masses were seen. The conversion factor from random plate variations to hadronic constant term was found using Lab E test beam data [3]. Fig. 15 shows the constant term as a function of rms light yield errors for several energies. A 2% constant term corresponds to 5% rms error.

6. EM Energy Resolution and e ID

There is a natural scale for electron energy resolution. The natural width of the Z is set by the electroweak coupling constant which is about 0.03.

$$\Gamma_Z / M_Z \sim \alpha_w \sim 1/30 \quad (2)$$

Therefore, the narrow Z width implies that the electron energy should be measured to better than 1% in order that the calorimeter not degrade Γ_Z .

The implication for a sampling calorimeter is that the absorber should be made as thin as is economically feasible. A thickness of 1/2 radiation length of Pb leads to a "stochastic term" coefficient of 12%. A match to this resolution would be to control all nonuniformities such that the constant term is $< 1\%$. Thus, for energies above 0.1 TeV, the constant term will dominate the energy resolution. The plate thickness is roughly proportional to the energy at which the resolution becomes constant.

6.1 Material Budget and Conversions

It makes little sense to construct a precise calorimeter and yet allow sufficient upstream material that the performance is degraded. This perception forces one to consider a maximum material "budget" upstream of the calorimeters. A glance at Table 2.1 shows that the rate of $\gamma + J$ above Pt of 20 GeV is ~ 40 Hz. If the γ converts upstream of the EM calorimeter, it looks like an isolated e. A 10% conversion probability gives a rate of 4 Hz for isolated e above 20 GeV, which swamps the isolated

electron trigger. Monte Carlo results [14] are given in Fig. 16. Indeed, photon conversions dominate all trigger sources for $P_t < 25$ GeV. This observation sets the conversion limit given in Table 2.2.

The issues for material budget also include e triggering and e ID. For example, the radiating e will deposit energy in several EM towers, effectively lowering the E_t below threshold for any single trigger tower. One also loses "isolation" as a criterion for e ID. The E/p cut may be compromised since the radiated energy is subtracted from p to form E . Finally, the match of the track to the SM centroid will be compromised. A study was made of the losses due to bremsstrahlung [14]. There are 2 effects; a failure to find the e track due to "kinks" and the mismatch of the track to the SM centroid. For 10% material, the e efficiency is reduced to $\sim 85\%$.

6.2 Massless Gaps and Upstream Material

The effect of inert material, t_i , placed directly in front of the EM calorimeter may be characterized as an additional term in the resolution.

$$dE/E = \left(a/\sqrt{E} \right) \left(e^{t_i/t_c} \right) \quad (3)$$

where $a = 0.019$ and the characteristic scale is $t_c = 1.58$ [15]. Thus, a scale is set for the material directly in front of the EM calorimeter, e.g. a magnet coil or a liquid argon cryostat. The "budget" for material distributed throughout, or upstream of, the tracking volume is considerably less as discussed in section 6.1.

In an attempt to alleviate that problem, one can sample the EM cascade directly behind the material using a "massless gap". Since the sampling fraction of the inert material is different from the EM calorimeter, one must weight this layer differently. For $t_i = 1$, the resolution for different energies and angles of incidence are shown in Fig. 17. Clearly, this amount of material is tolerable in that the resolution is not badly degraded. Note also that the optimal weight of the layer is not strongly energy or angle dependent. The flat plate geometry means that dE/E scales as a/\sqrt{ET} .

6.3 Higgs $\rightarrow 2 \gamma$ and Resolution

The most stringent limit on resolution is set by the desire to study the 2γ decay mode of a light Higgs. The natural width is effectively zero. Therefore, since there are considerable backgrounds, the maximization of the S/N ratio argues for the best possible resolution. A plot of the mass distribution for a typical sampling calorimeter is shown in Fig. 18.

Note that the desire to observe the 2γ decay mode implies a very good photon ID cleanliness. For example, a glance at Table 2.1 shows that the JJ rate is ~ 1 Mhz, while the 2γ rate is ~ 0.4 Hz. Therefore, a J/γ rejection of ~ 1000 is implied if the 2γ mode is to be cleanly identified. The desire for excellent resolution must be moderated by the realization that there are systematic effects. The calorimeter is an ensemble of towers which must be kept uniform. It is assumed that the "constant term" will be kept to $< 1\%$ throughout this ensemble.

6.4 Uniformity Tolerance in Sampling Calorimeters

An example of the type of errors which must be kept under control is the variation in plate thickness of a sampling type calorimeter. A study [3] was made of the relationship between the EM resolution and the rms plate thickness variation. As seen in Fig. 19, a plate thickness tolerance rms of 2% induce a constant term of 1/2%. The effect is again essentially energy independent and linear in the rms light yield error.

Note that this specification on thickness tolerance assumes that each tower is not separately calibrated. If it were, then one has effectively measured the plate thicknesses near shower maximum, and the tolerance can be relaxed. Monte Carlo studies show that the limit can be relaxed by a factor $\sim 2/3$. Note also that thinner plates make one less sensitive to plate variations since the shower is spread over several plates, and individual plate errors are then "washed out".

6.5 Speed and Pileup, High Luminosity

The issue of pileup is perhaps most severe for the EM calorimetry since the e ID requires a variety of cuts. For example, the rate for JJ and $q\bar{q}$ with $Q \rightarrow q_{\text{ev}}$ is in the ratio of 1,000,000 for $M \sim 100$ GeV. Therefore, J/e rejection factors of that order are desired.

The e ID cuts are typically EM/HAD, "isolation", and SM track match. For a density, ρ , of 10 particles per unit of rapidity, each with $\langle Pt \rangle \sim 0.7$ GeV, there is ~ 1 GeV of E_t per unit of area, A , in η - ϕ space. For the SSC with luminosity, L , of $10^{34}/(\text{cm}^2\cdot\text{sec})$ there are 16 interactions per bunch. For a calorimeter with 20% stochastic term and 1% constant term, studying e from Z over a 2×2 set of towers (for transverse containment), one needs towers < 0.16 not to degrade resolution with pileup for the fastest calorimetry imaginable.

Resolution is not the entire story. Studies [16], have shown that, for a 50 GeV E_t e from $Z \rightarrow ee$ decays, $EM/HAD > 10$ and (isolation E)/ $EM < 1/10$ will, at a luminosity of $L = 10^{34}/(\text{cm}^2\cdot\text{sec})$, and 0.05 segmentation lead to a 8% e efficiency loss. In addition, the track match cut will suffer with increased luminosity. The results in Fig. 11 may be crudely scaled with $10 \times$ luminosity increase by the square root. This means that, for the same criteria, the SM strip length cannot exceed ~ 0.15 .

7. Summary

Various parameters having to do with the position, energy, and time measurements of calorimeters are defined with respect to physical processes of interest at SSC/LHC energies. Design criteria are thus defined.

References

1. E. Eichten, et al., *Rev. Mod. Phys.* **56** 4, 579 (1984).
2. *SDC Calorimeter Design Requirements*, J. Siegrist ed. August 5, 1991.
3. *Calorimeter Conceptual Design - Tile/Fiber Scintillator Option*, ed. SDC Tile/Fiber Calorimeter Group, September 3, 1991.
4. D. Green, et al., *Depth Requirements in SSC Calorimeters*, Fermilab-FN-570, August 1991.
5. L. Jones, *Reduction of Calorimeter Depth by Weighting Last Layer*, UM HE 91-27.
6. J. Hauptman, *Fake Missing ET Trigger Rates Due to Non-Hermeticity, Finite Energy Resolution and Finite Depth*, SDC Note.
M. Barnett and Ian Hinchliffe, *The Impact of Resolution, Cracks and Beam Holes on Detection of Processes with Missing Energy*, SSC-SDE-29, LBL-28773, March 28, 1990.
7. A.B. Wicklund, *b-Jet Tagging Using Electrons at SDC*, August 14, 1991, SDC-91-0051.
8. *Letter of Intent* by the Solenoid Detector Collaboration, November 30, 1990, SDC-90-00151.
9. T. Kirk, A.B. Wicklund, SDC-91-00018, April 11, 1991.
10. D. Green, A. Para, *Radiation Damage, Calibration and Depth Segmentation in Calorimeters*, Fermilab-FN-565, May 1991.
11. A. Para, et al., *Jet Energy Resolution of the SDC Detector*, Fermilab-TM-1270.
12. D. Green, *Dijet Mass Resolution and Compensating Calorimetry*, Fermilab-TM-1740.
13. D. Green, *Dijet Spectroscopy at High Luminosity*, Fermilab - Conf 90/151.
14. Report of the Task Force on Impact of Material in Tracking Volume, SDC.
15. D. Green, *Effect of Inert Material on Z1 Mass Resolution for $H \rightarrow ZZ \rightarrow eee$* , Fermilab-TM-1736.
16. J. Colas, et al., *Calorimetry at the SSC*, DESY 90-136.

TABLE 2.1 RATES AT SSC FOR DESIGN LUMINOSITY



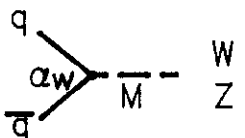
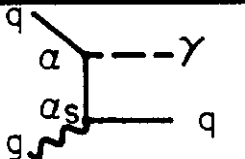
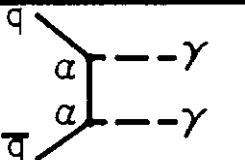
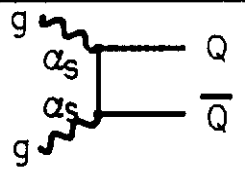
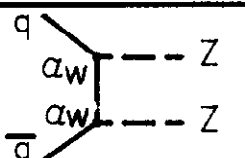
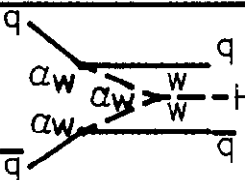
PROCESS	DIAGRAM	$\frac{dR}{d\eta dP_t}$ (Hz/GeV)	$\frac{dR}{d\eta}$ (Pt>20GeV)
JETS		$25,000 (20/P_t)^3$	1,000,000
π^0		$100 (20/P_t)^3$	4000
W,Z		$P_t \sim M/2$	40(W) 12(Z)
γ		$1.0 (20/P_t)^3$	40
$\gamma\gamma$		$0.01 (20/P_t)^3$	0.4
$Q\bar{Q}$		$\frac{d\sigma}{dP_t^2} \sim \frac{\sigma/MQ^2}{[1+(\frac{P_t}{MQ})^2]^2}$	$8 (\frac{100}{MQ})^3$
WW	FROM $t \bar{t}$	$\frac{d\sigma}{dP_t^2} \sim \frac{\sigma/MQ^2}{[1+(\frac{P_t}{MQ})^2]^2}$	$8 (\frac{100}{MQ})^3$
ZZ			4×10^{-3}
H(1 TeV)			2×10^{-4}

TABLE 2.2 PHYSICS REQUIREMENTS FOR CALORIMETER PARAMETERS

PARAMETER	PROCESS	ALLOWED RANGE
HERMITICITY	JJ	J MISIDENTIFICATION $<10^{-3}$
CALIBRATION	Z	$(Pt)_e \gtrsim 20\text{GeV}$ TRIGGER
UPSTREAM(COIL) MATERIAL(TRACK)	Z, Γ_Z ISOLATED e TRIGGER	$\lesssim 1 X_0$ FOR COIL $\lesssim 0.1 X_0$ FOR TRACKING
SPEED	$Z \rightarrow JJ$ $Z \rightarrow ee, \text{PILEUP}$	$\lesssim 1$ BUNCH CROSSING
ANGULAR COVERAGE	ZZ $\hookrightarrow \nu \bar{\nu}$	$ \eta \lesssim 3, \epsilon_e$ $ \eta \lesssim 5, Z+J$
TRIGGER COVERAGE	ZZ	$(Pt)_e \gtrsim 20\text{GeV}$
TOTAL DEPTH	$M_{JJ} = 10\text{TeV}$	$D \gtrsim 10$
LONGITUDINAL h SEGMENTATION	p_T IN JJ	D1,D2 FOR h
LONGITUDINAL EM SEGMENTATION	$Z \rightarrow ee$	RADIATION DAMAGE 2 DEPTH SEGMENTS FOR EM AT LARGE $ \eta $
EM RESOLUTION HADRON RESOLUTION	$Z \rightarrow ee, \Gamma_Z/M_Z$ ($\alpha_W/\pi \approx 0.01$) M_{JJ}	$0.2/\sqrt{E} \oplus 0.01$ OR BETTER $0.7/\sqrt{E} \oplus 0.03$ OR BETTER
COMPENSATION	M_{JJ}	$ e/h-1 < 0.3$
TRANSVERSE h SEGMENTATION	$H \rightarrow ZZ$ $\hookrightarrow JJ$ $t \rightarrow Wb$ $\hookrightarrow ce\nu$	$\Delta\eta_h < 0.05$ $\Delta\eta_h < 0.05, \text{EM/HAD}$ ISOLATION
TRANSVERSE EM SEGMENTATION	$H \rightarrow ZZ$ $\hookrightarrow JJ$ $t \rightarrow Wb$ $\hookrightarrow ce\nu$	$\Delta\eta_e < 0.05$ J REJECTION e EFFICIENCY

Figure Captions

- 1.a Acceptance for Higgs bosons of mass $M = 0.2, 0.4, 0.6$ and 0.8 TeV as a function of the rapidity coverage. All 4 leptons in the $H \rightarrow ZZ \rightarrow 4e$ decay chain must have $\eta < \text{the cut}$.
- 1.b As in a, except the cut variable is the minimum P_t which each e must have. The pseudorapidity is $|\eta| < 2.5$.
2. Cross sections for WW production via $t\bar{t}$ formation and cross sections for direct production of WW and WZ pairs.
3. Relative cross sections for ZZ and ZJ with J falling outside the fiducial volume of the calorimeters.
4. Fractional dijet mass resolution for 10 TeV dijets as a function of depth, D. The points correspond to different parametrizations of data, CCFR data, \bullet , WA1 data, \circ , and Lab E data, \square .
5. Measured energy distribution for 0.45 TeV beam incident on a calorimeter.
 - a. $D = 10.1$, unweighted
 - b. $D = 8.70$, unweighted
 - c. $D = 10.1$, weighted by 3
 - d. $D = 8.70$, weighted by 3
6. Distribution of fraction of contained energy, f , for 0.45 TeV test beam data.
 - a. All events with $D = 10.1$
 - b. Longitudinal segmentation with $D_2 = 3.5$, $D_1 = 6.6$ and ratio of energy in D_2 to total less than 0.18.
7. Fractional mass resolution for $Z \rightarrow JJ$ for low P_t Z's, Θ , and boosted Z with $P_t = 0.55$ TeV, \square , as a function of tower transverse segmentation.
8. Magnitude of the "induced" constant term due to damage coefficient of 0.1, 0.3, and 0.5 as a function of electron energy.
 - a. No correction.
 - b. Corrected using simple energy independent form derived from 2 longitudinal EM compartments.
9. Study of isolation for $t\bar{t}$ events with subsequent $t \rightarrow Wb$, $b \rightarrow c\bar{c}\nu$ decays. The ratio of average electron energy to total EM + h energy in a cone of radius R as a function of R.
10. The mean deviation between the SM centroid and the exact tracking position as a function of strip length for $t \rightarrow Wb \rightarrow c\bar{c}\nu$ events. Strip width is 0.01. Points are \bullet , field on and \circ , field off $\times 1/10$. The solid curve is square root (length). The dashed curve is to guide the eye through the data. The shaded portion corresponds to the region where the matching error is $> 1/2$ the strip width.
 - a. azimuthal strips
 - b. strips in rapidity

11. The fractional mass resolution for Z and 1 TeV Z' decays into dijets.
 - a. Perfect detector, no underlying event, finite cone $R = 0.7$.
 - b. Perfect detector, underlying events
 - c. As in b but with $0.15/\sqrt{E} \oplus 0.01$ for EM and $0.3/\sqrt{E} \oplus 0.02$ for HAD
 - d. As in c but with $0.5/\sqrt{E} \oplus 0.03$ for HAD
 - e. As in c but with $0.7/\sqrt{E} \oplus 0.04$ for HAD
 - f. As in d but with $0.25/\sqrt{E} \oplus 0.02$ for EM
 - g. As in d but with $e/h = 1.3$ for HAD
12. Dijet mass resolution as a function of mass. The "data points" refer to the total error. The points, \bullet , refer to fragmentation and underlying event fluctuations, \circ , refer to calorimeter resolution, and ∇ refer to neutrino fluctuations.
13. Dijet mass resolution as a function of mass. The data points are for the "baseline" SDC calorimeter, \bullet , a calibrated calorimeter with $e/h = 1.3$, \circ , and a calorimeter with $e/h = 1.3$ which is only calibrated at asymptotic energies, ∇ .
- 14.a Plot of standard deviation of δ as a function of R for H(800) events keeping only tracks with $k_t > 1.0$ GeV with no additional overlap events (solid), 8 overlap events (dashed), and 16 overlap events (dot-dashed). The results using only W fragments are shown as \circ symbols.
- 14.b As in Fig. 15a except that only tracks with $k_t > 2.0$ GeV are allowed.
15. Induced constant term as a function of rms light yield for a hadron calorimeter. Test beam data from the "Lab E" spectrometer were used at beam energies of 0.1, 0.2, and 0.45 TeV.
16. Differential cross section as a function of P_t for leptonic W decays, semileptonic t decays, and photon conversions.
17. Fractional energy resolution for an EM calorimeter with $t = 1/2$ samples preceded by $t_i = 1$. The results are for \bullet , 25 GeV, $\theta = 90^\circ$; \circ , 25 GeV, $\theta = 30^\circ$; $[\]$, 50 GeV, $\theta = 90^\circ$.
18. Two γ mass distribution for W + H events with $H \rightarrow 2 \gamma$ for the parameters of the SDC detector.
19. Induced constant term as a function of rms light yield for a EM calorimeter. EGS Monte Carlo "data" were used at incident energies of 10 and 50 GeV.

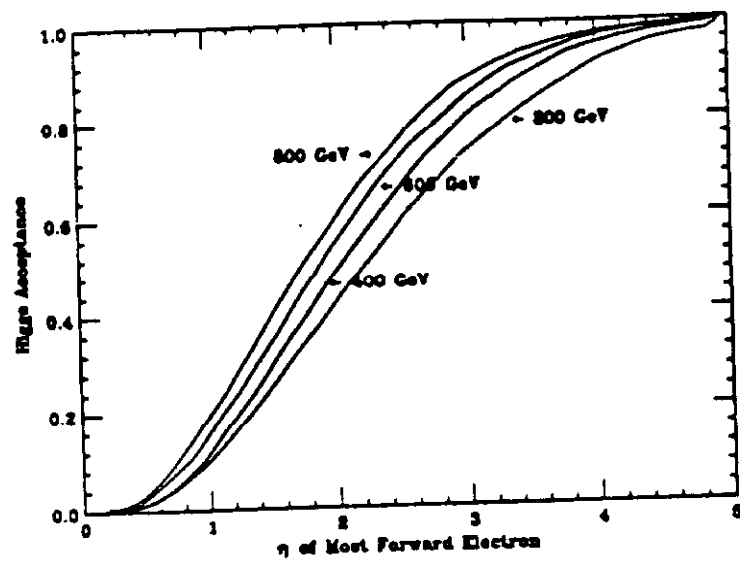


FIGURE 1.a

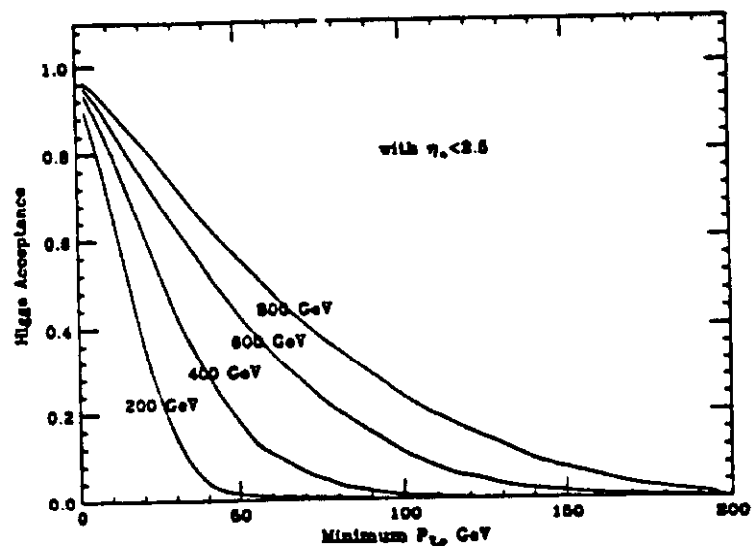


FIGURE 1.b

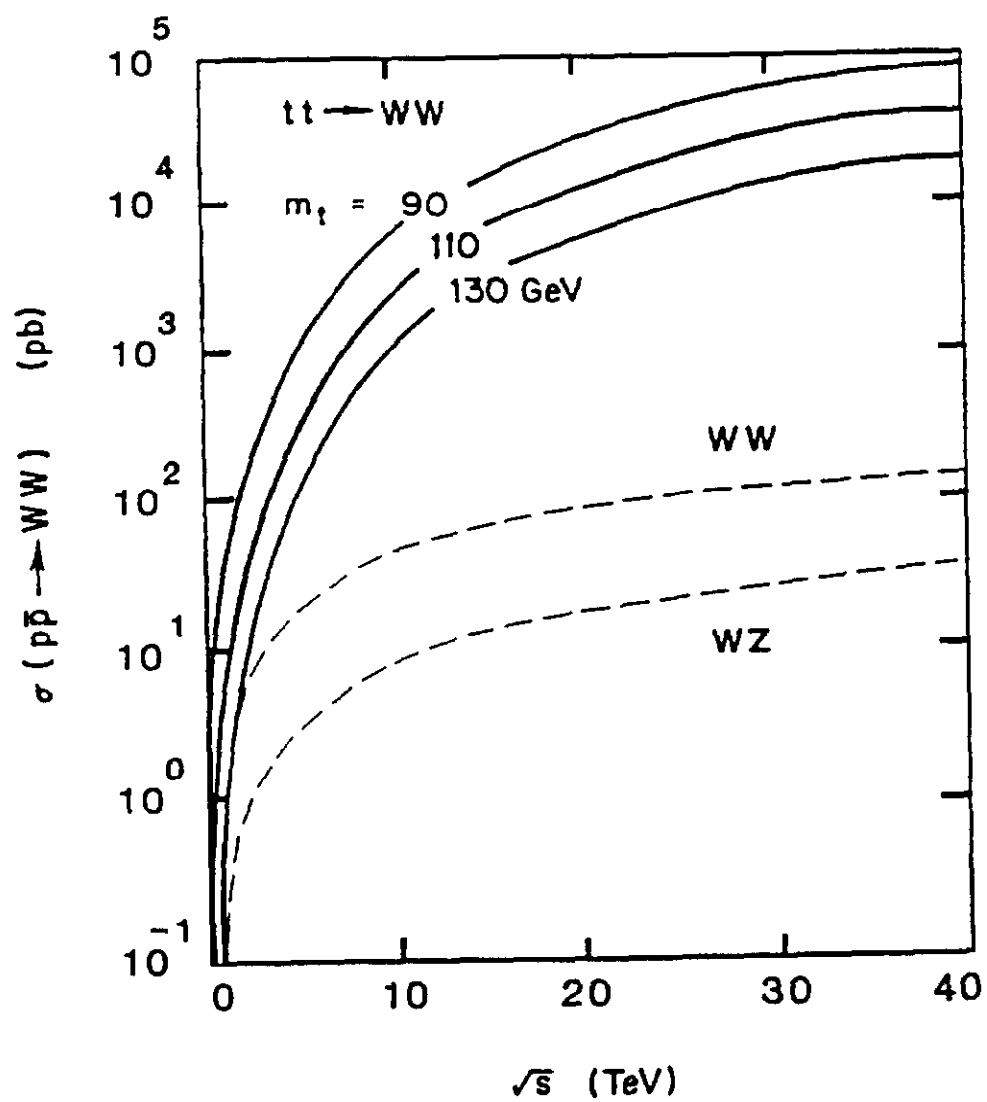


FIGURE 2

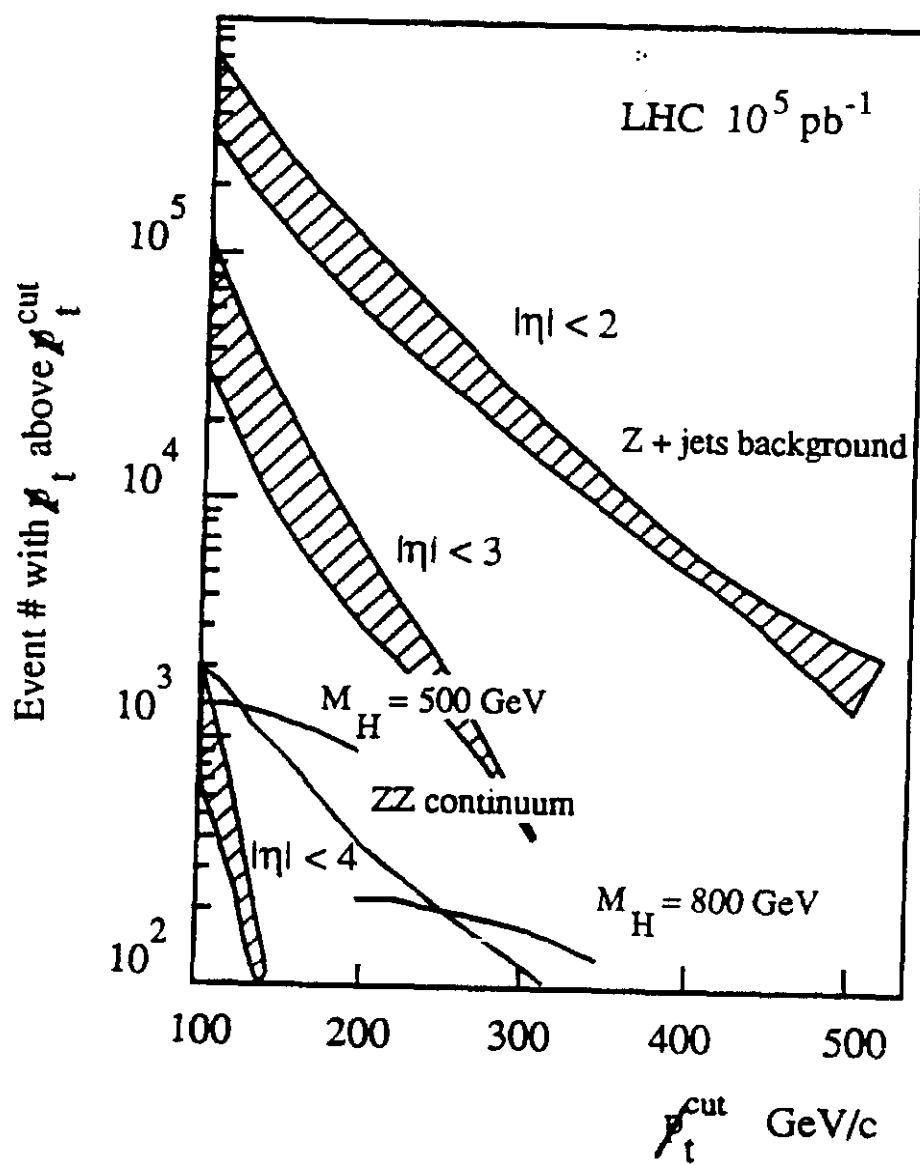


FIGURE 3

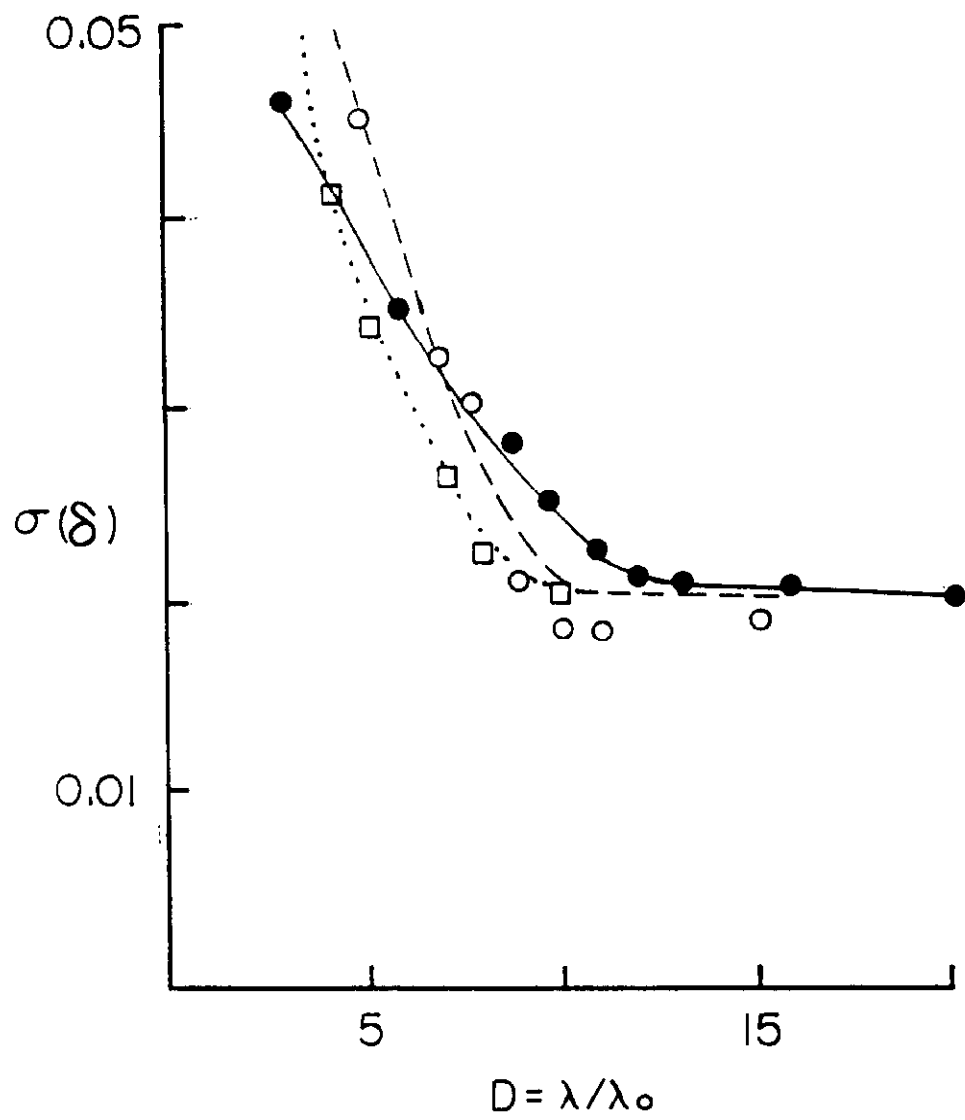


FIGURE 4

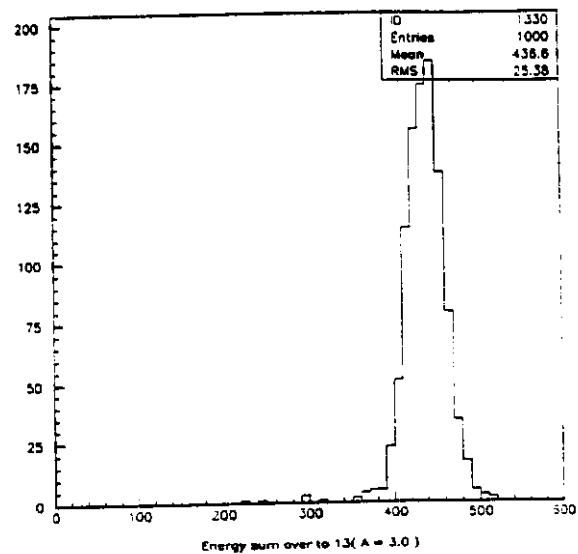
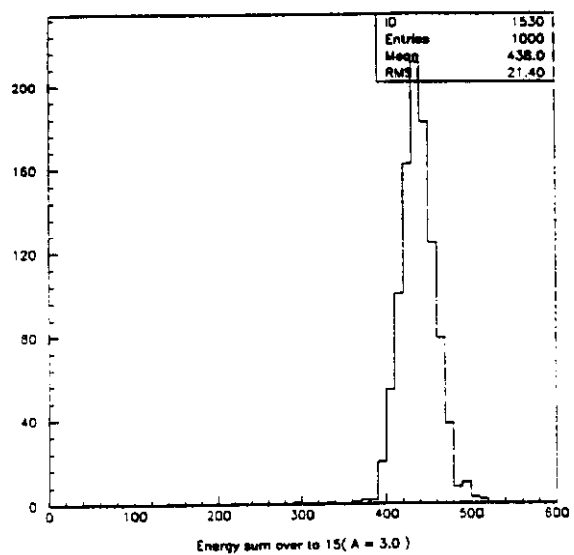
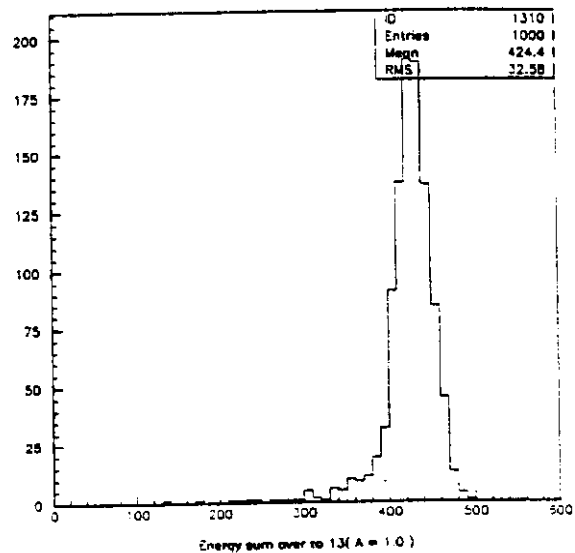
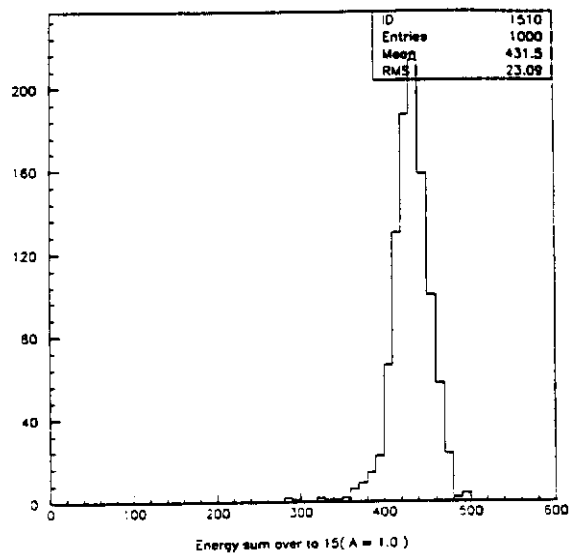


FIGURE 5

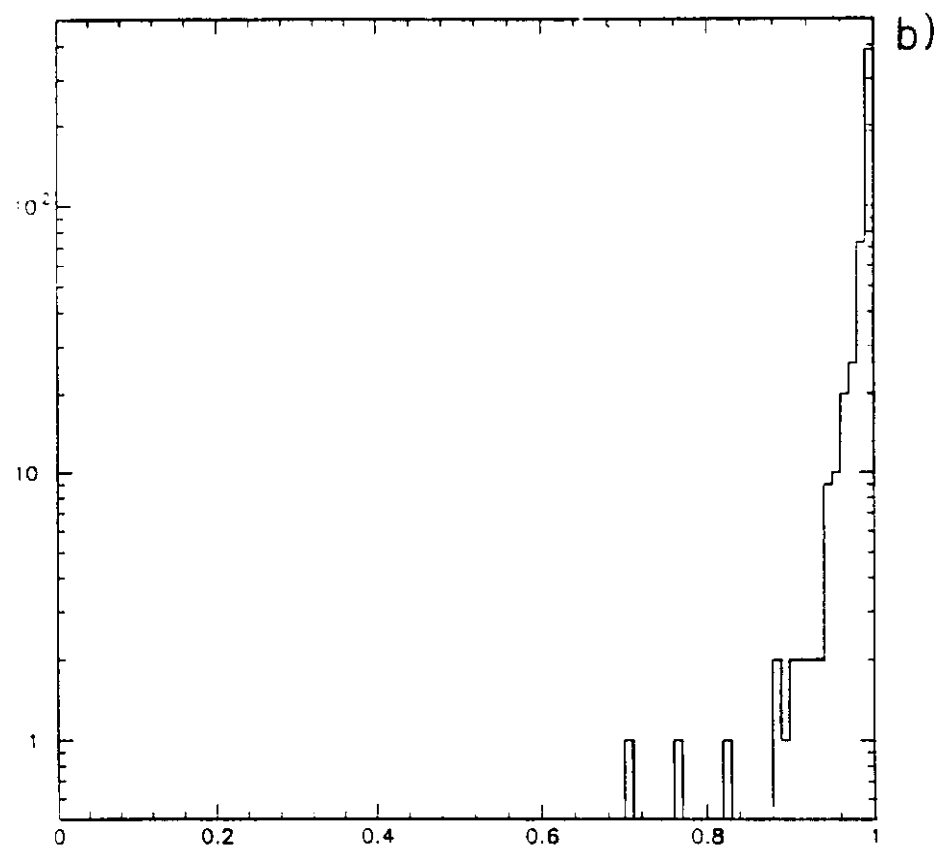
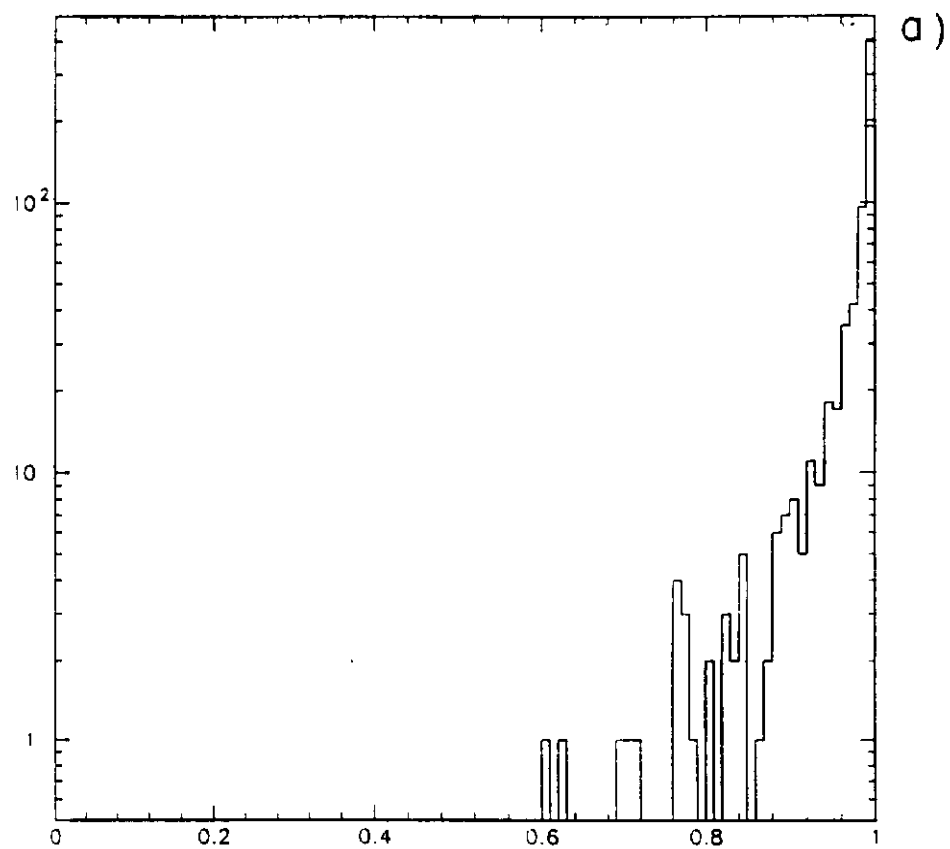


FIGURE 6

f

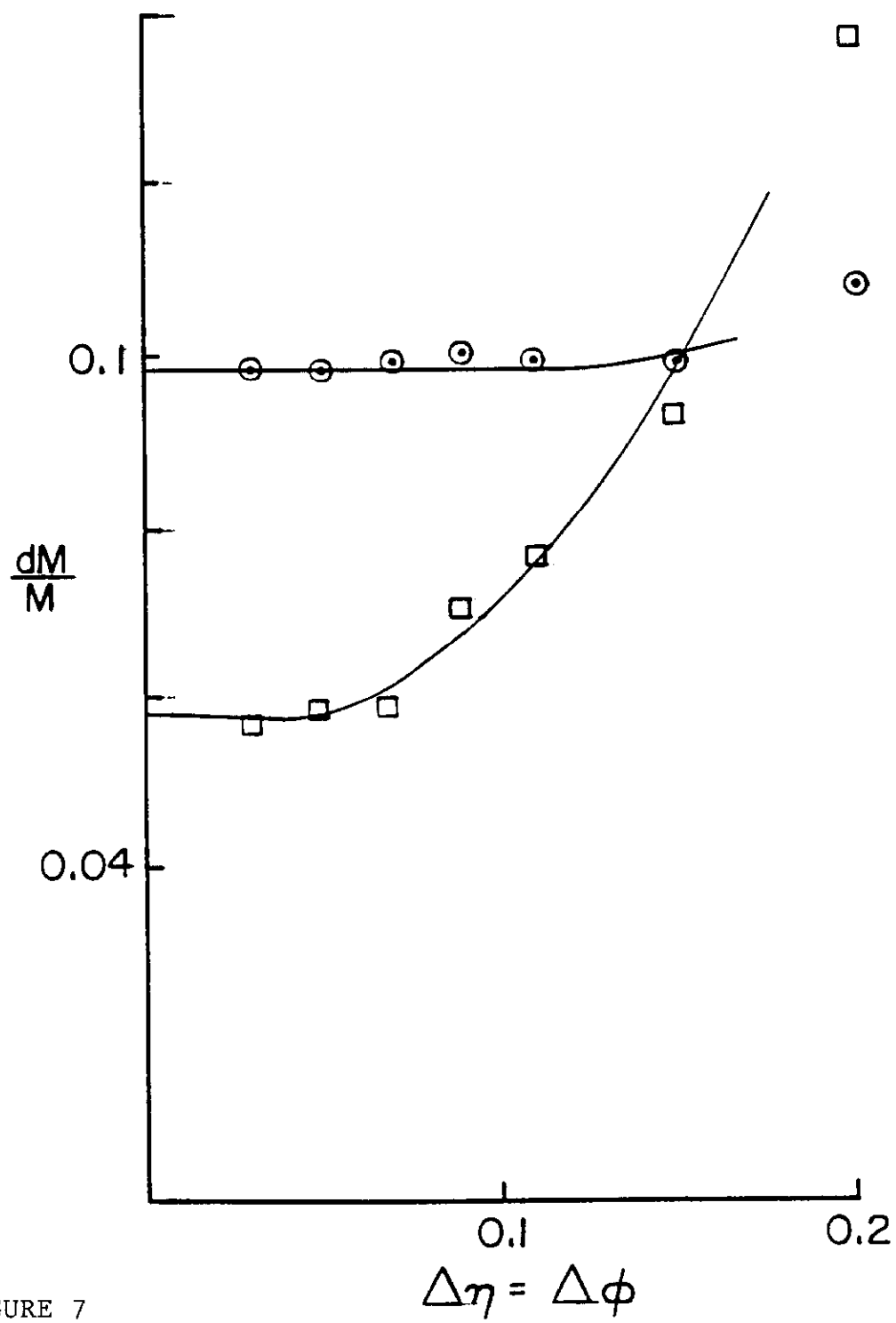


FIGURE 7

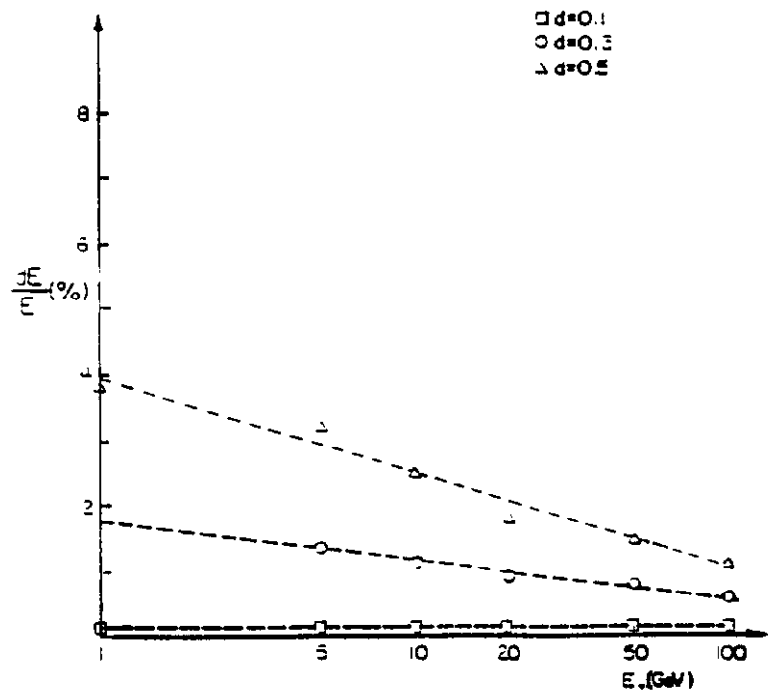
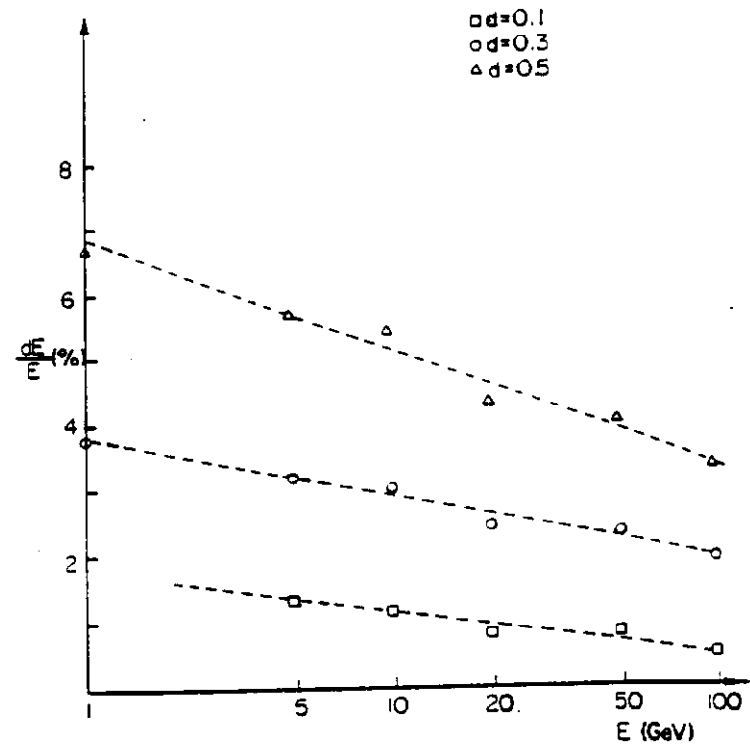


FIGURE 8

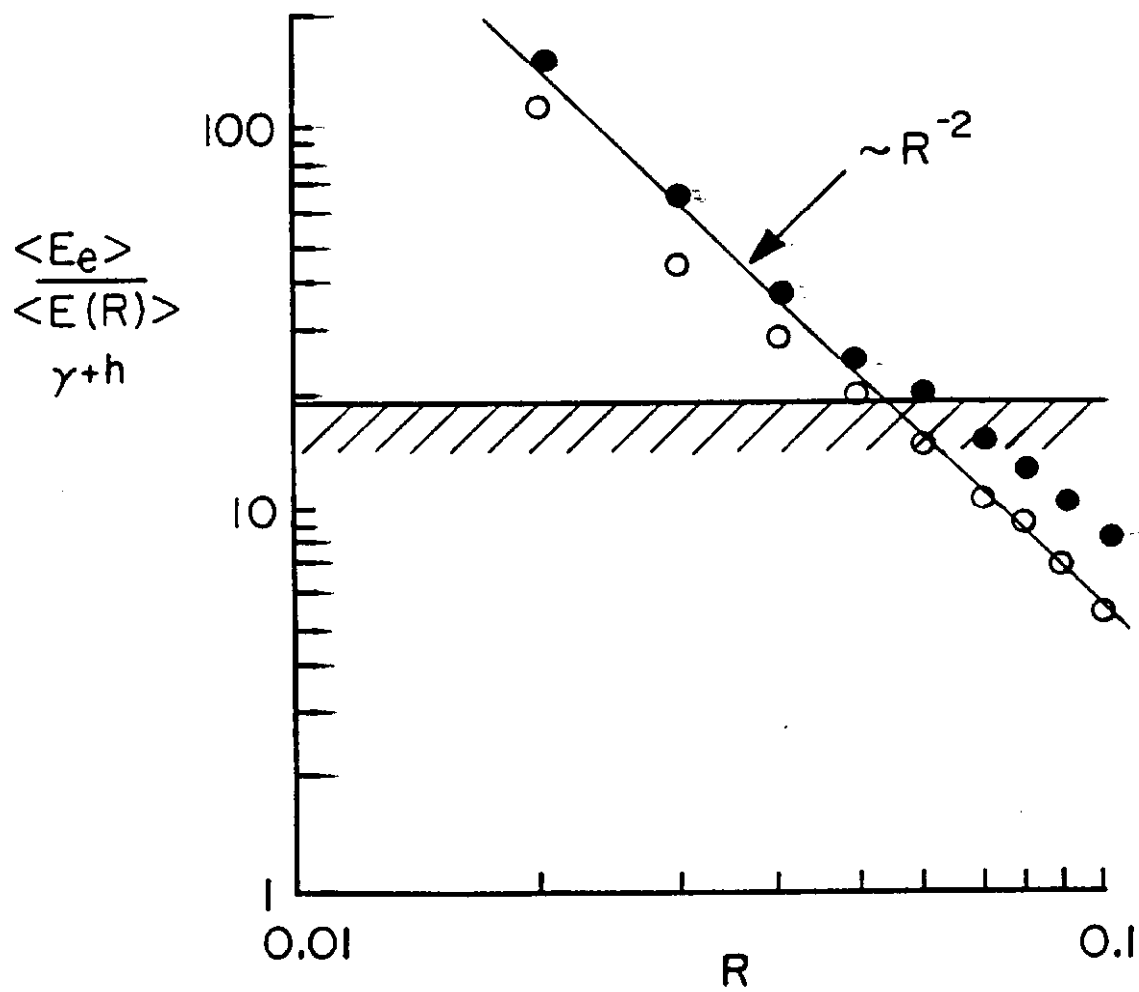


FIGURE 9

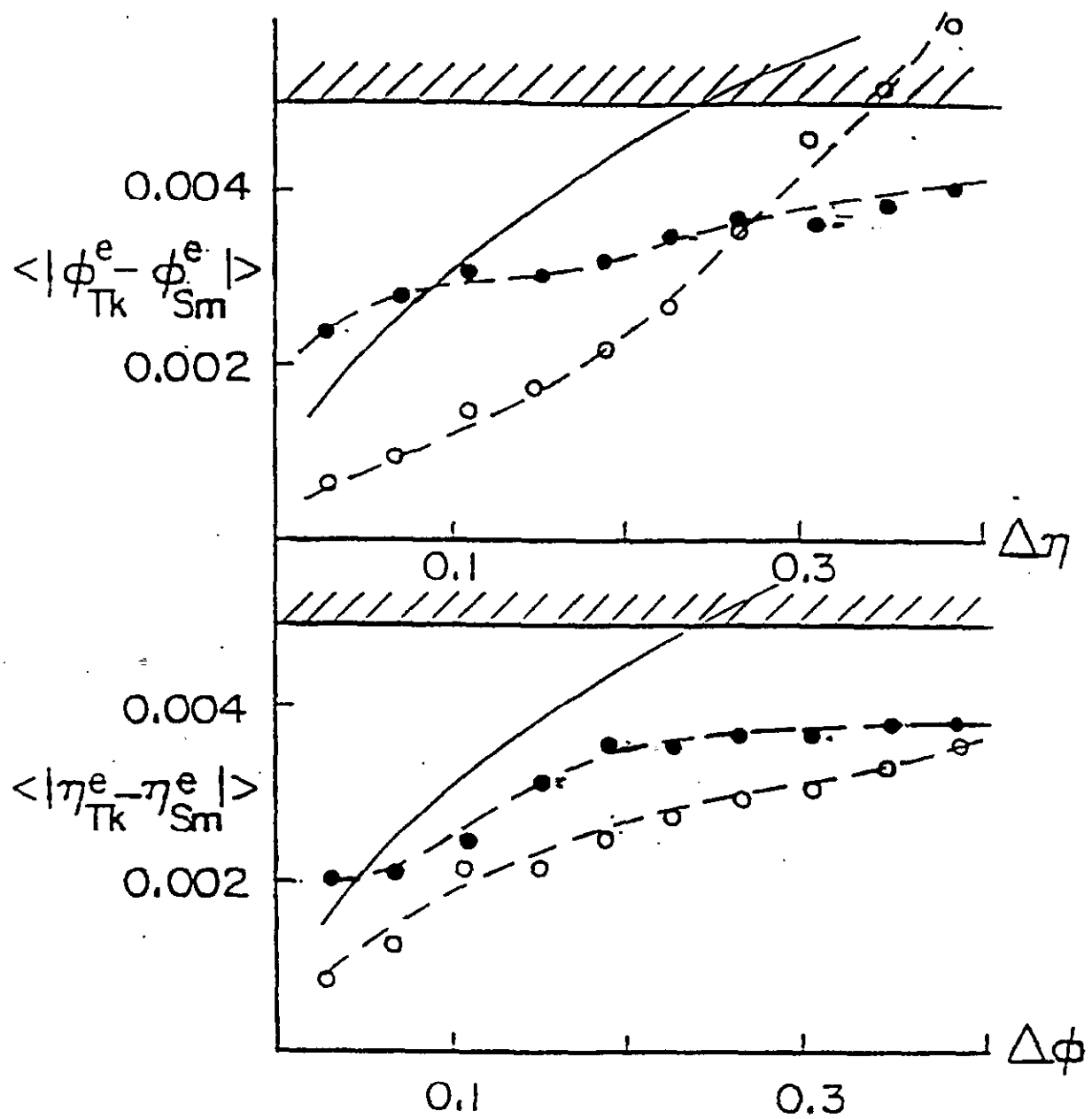


FIGURE 10

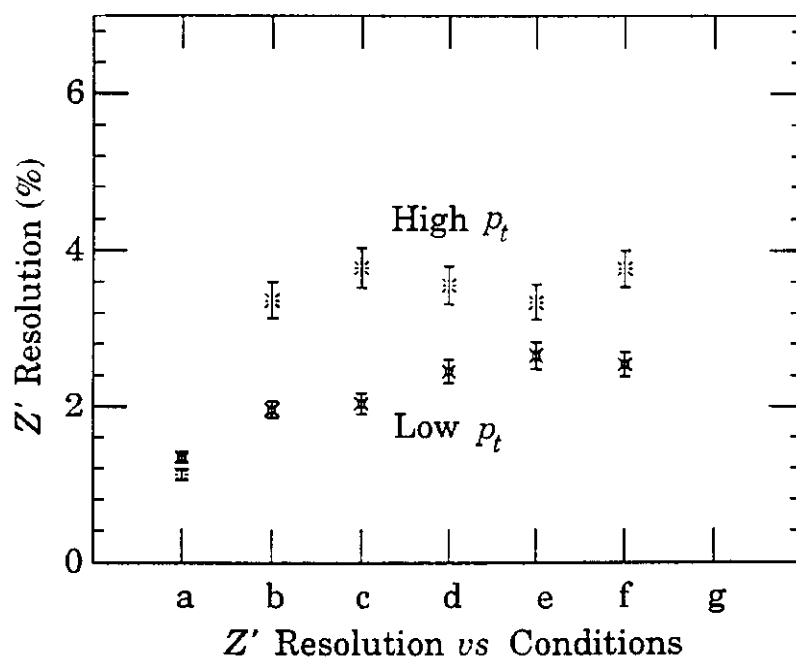
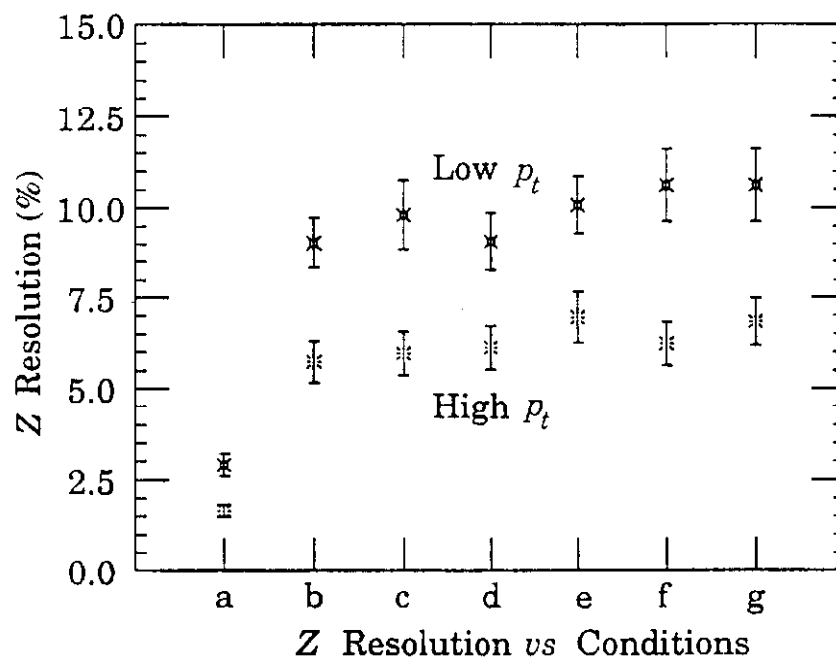


FIGURE 11

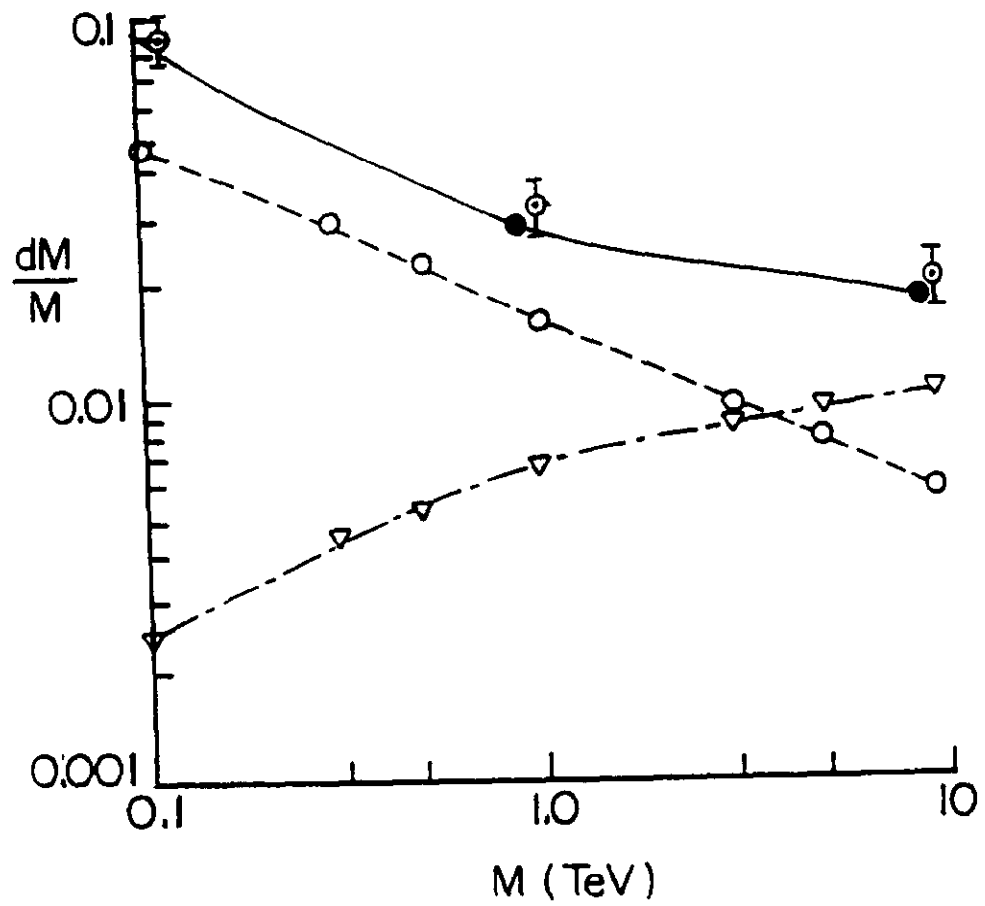


FIGURE 12

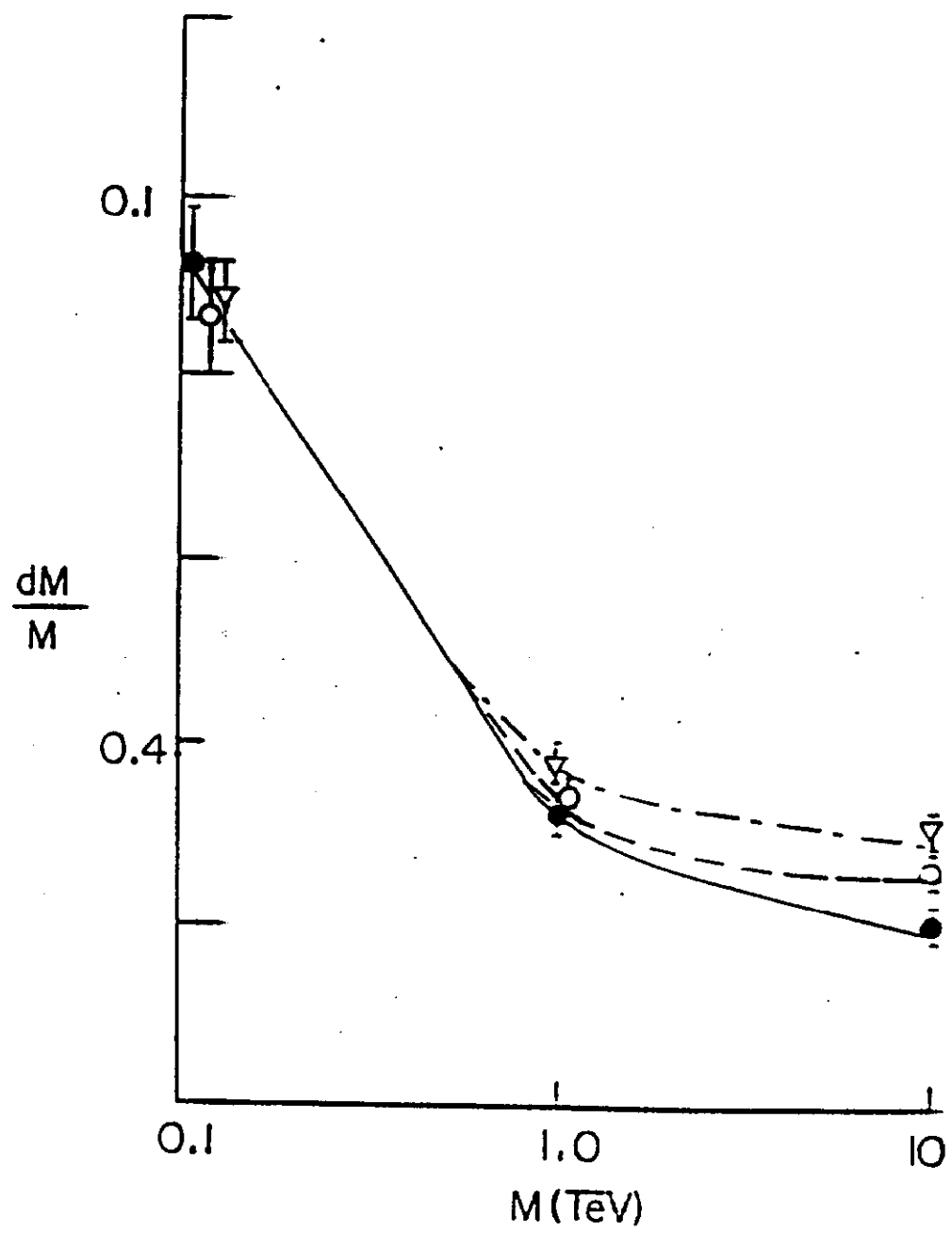


FIGURE 13

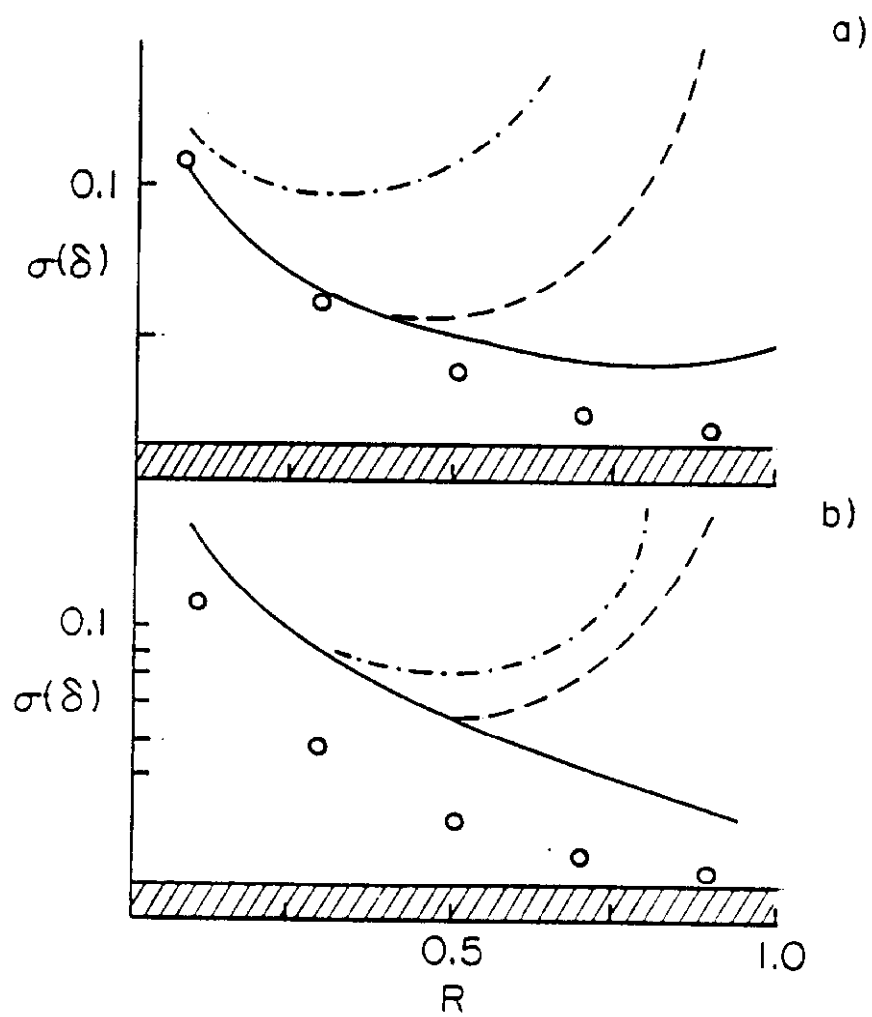


FIGURE 14

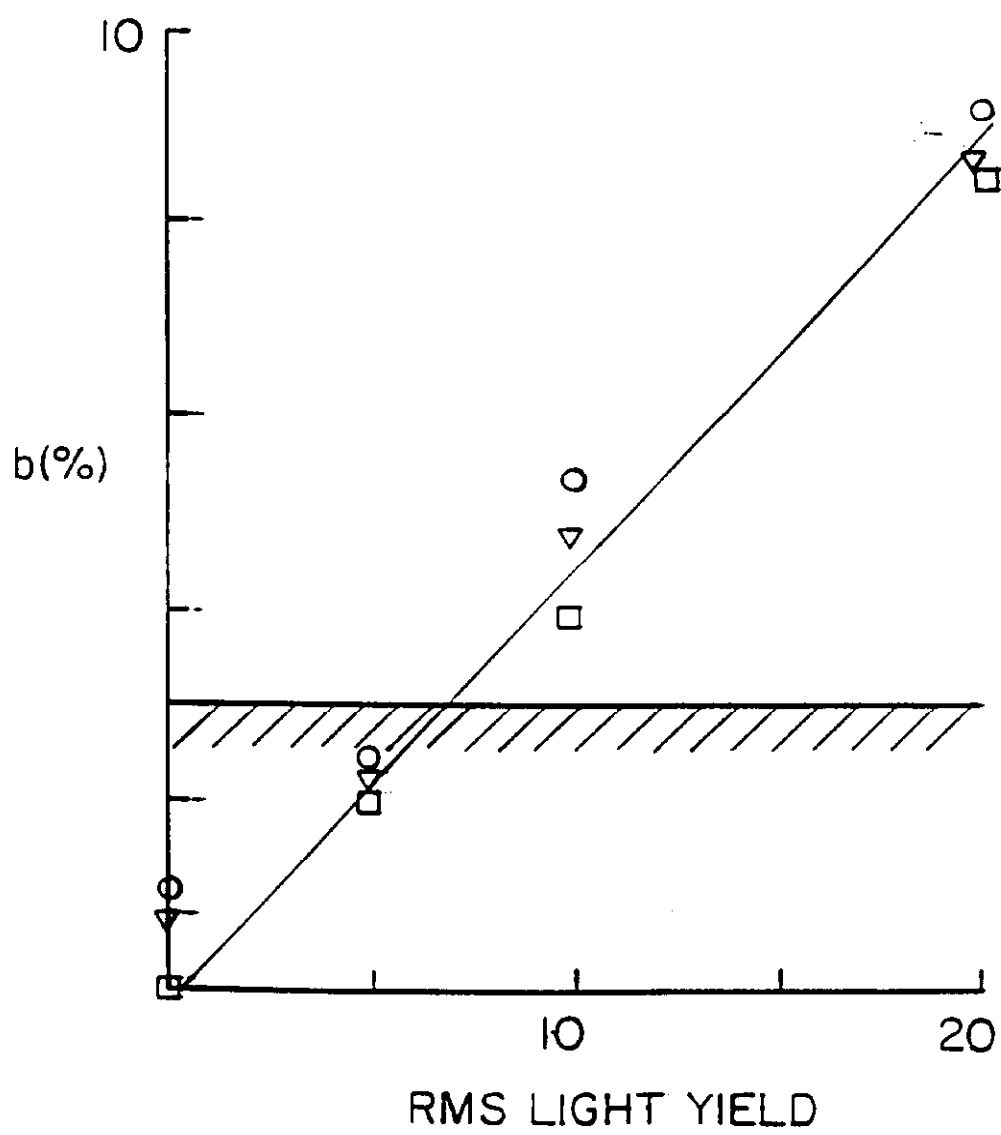


FIGURE 15

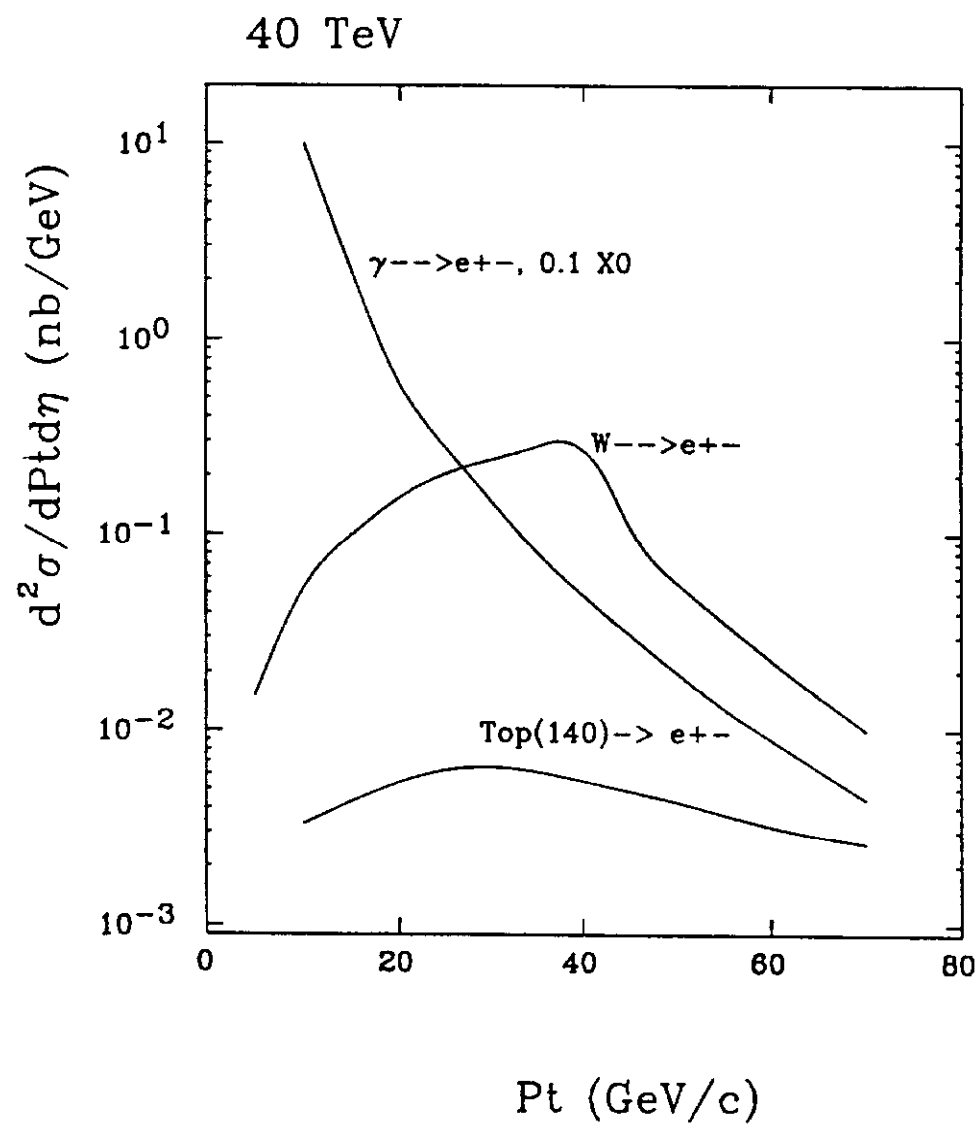


FIGURE 16

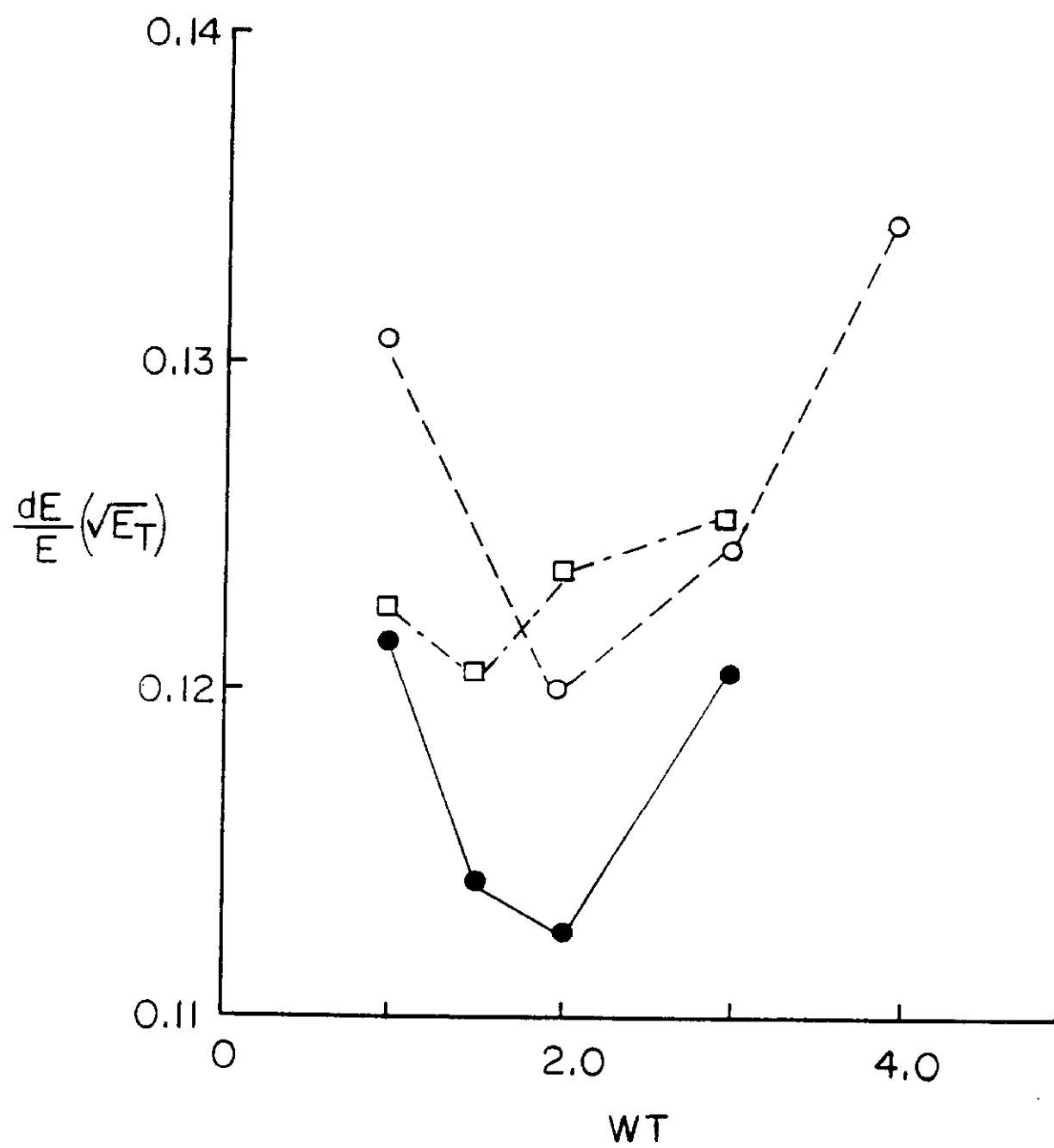


FIGURE 17

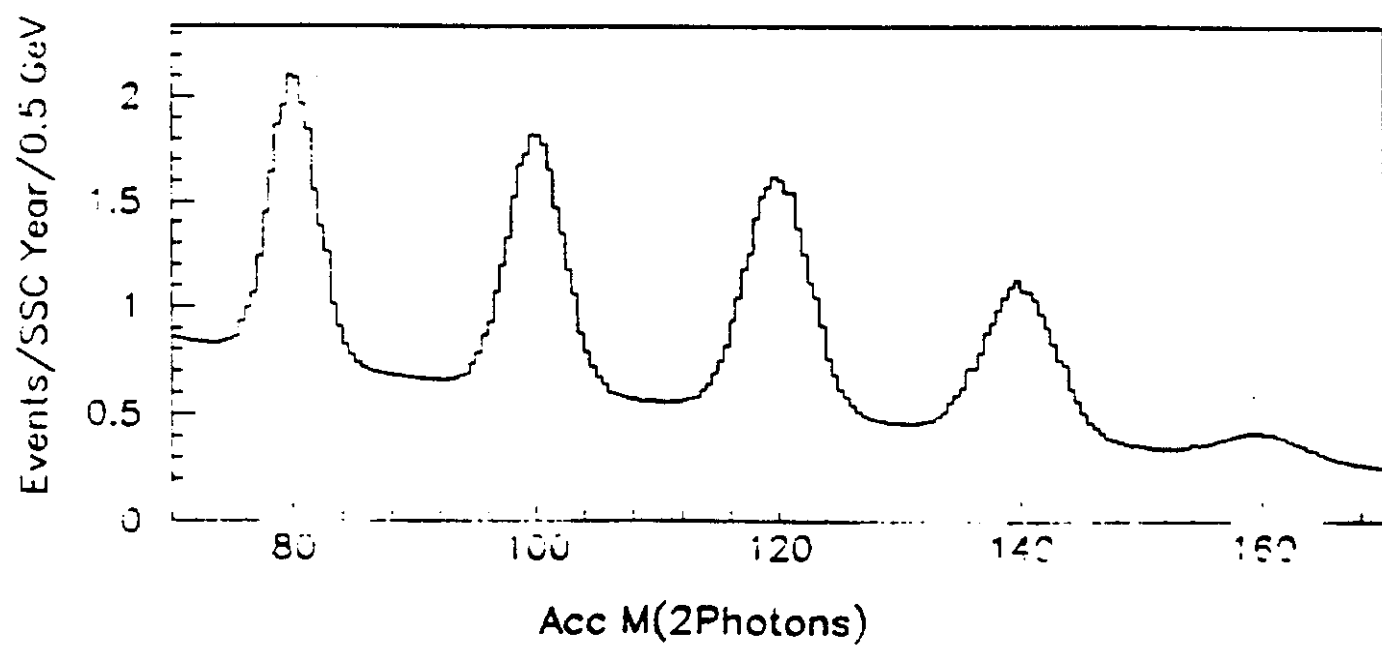


FIGURE 18

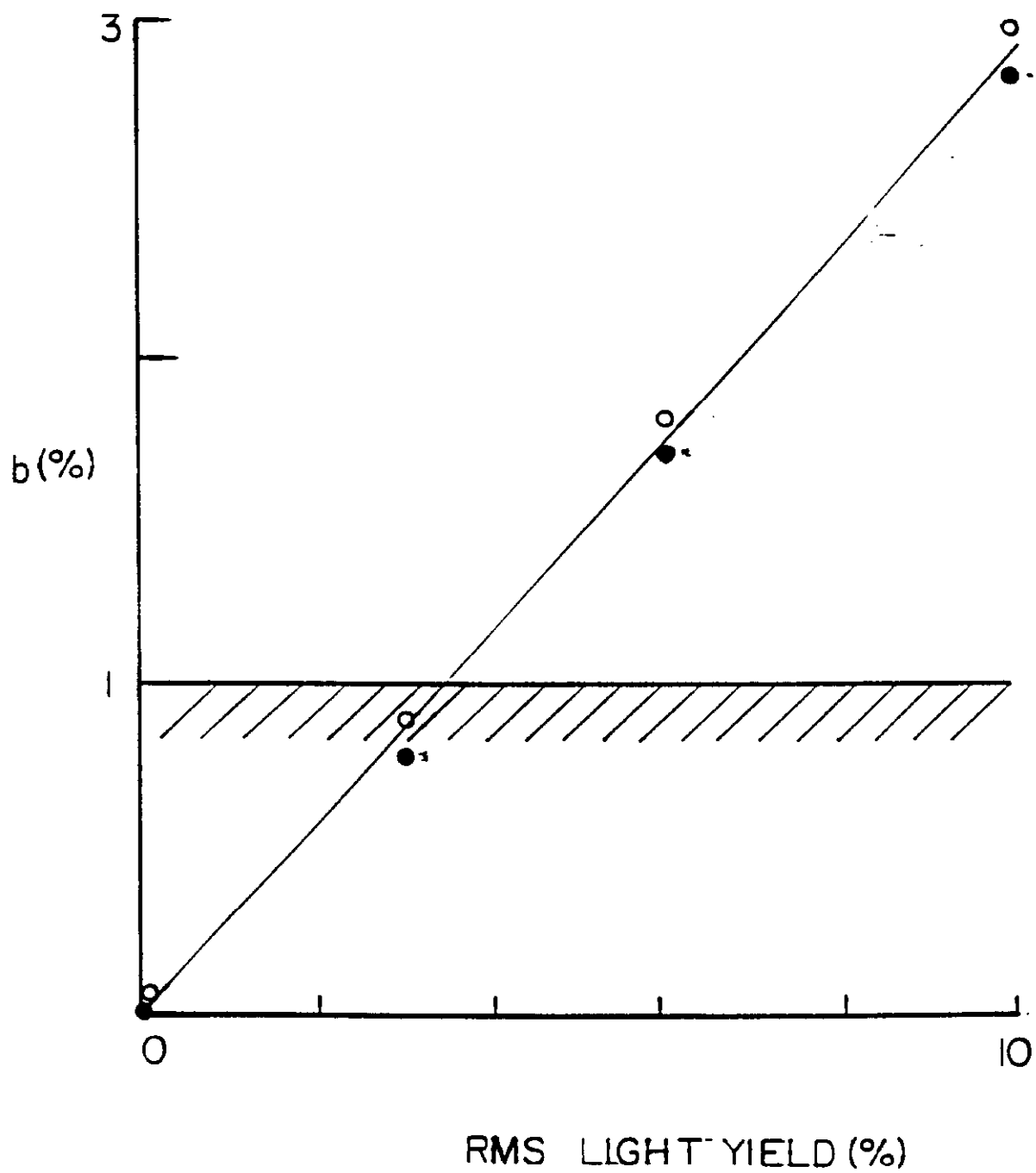


FIGURE 19